Superconducting Current Transformer for Testing Nb_3Sn Cable Splicing Technique

N. Andreev, E. Barzi, S. Bhashyam, C. Boffo, D. R. Chichili, S. Yadav, I. Terechkine, A.V. Zlobin

***Abstract*—To provide a quick feedback on different approaches to superconducting cable splicing design and assembly techniques, a superconducting current transformer that can deliver more than 20 kA for testing splice samples was designed and fabricated. The existing infrastructure of the Short Sample Test Facility at Fermilab, including its cryostat, power supply, and data acquisition system, was used for housing and operating the transformer. This report presents the design features of the transformer and the main results of cable splice tests.**

***Index Terms*—current transformer, dipole magnets, Nb_3Sn cable, superconducting magnets.**

I. Introduction

Test results of several Nb_3Sn dipole magnets at Fermilab have shown that, among other possible reasons, cable splicing could be a weak point of the chosen fabrication technique. Most of the observed quenches took place in the Nb_3Sn cable in the vicinity of the coil lead splice [1]**.** A strain of the cable strands was suspected to be a major factor leading to cable performance degradation although other possible factors were also considered. A new design of the coil lead end and splice area as well as a lead splicing procedure that prevent cable strands from being deformed at every stage of the magnet assembly have been developed. To make a quick turn-around while testing the new design and technological approaches, a compact superconducting current transformer (SCT) was designed, fabricated, and tested. The Fermilab's Short Sample Test Facility (SSTF) with the existing cryostat and test infrastructure was used to house the transformer [2].

This paper presents the transformer design, results of its commissioning, performance limit measurements, and summarizes the main results of cable splice tests.

II. SC Current Transformer Design

The electromagnetic design concept of the SCT was similar to that used earlier for similar purposes [3],[4]. The existing SSTF cryostat, that was used to house the transformer, imposed some limitations on the transformer performance. The schematic of the transformer is shown in Fig. 1. The transformer cross-section with major dimensions is shown in Fig. 2. The primary multi-turn coil is placed inside the secondary single-turn winding. The secondary winding consists of two U-shaped parts: a regular NbTi cable section placed close to the primary coil for better magnetic coupling, and a removable cable section modeling splice area. During testing, pre-shaped and reacted removable section was inserted into the regular part of the secondary winding and spliced with the NbTi cable. After testing, this section could be removed and new samples could be inserted without disassembling the transformer.

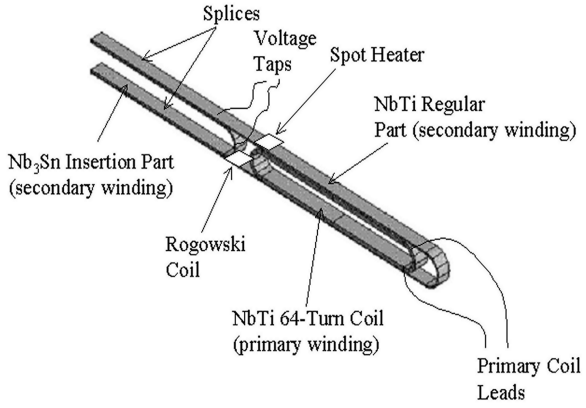

Fig. 1. The superconducting current transformer general schematic.

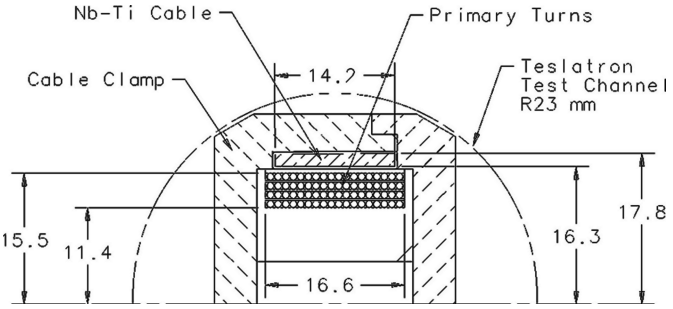

Fig. 2. Transformer cross-section (all dimensions are in mm).

The primary turns of the transformer were wound on a G-10 core using 0.8-mm NbTi strand (SSC inner layer strand) coated with 50-μm polyimid insulation. The number of turns in the primary coil is 64. The regular part of the secondary winding was made of Rutherford-type NbTi cable similar to that used for making current leads in the dipole models (27 strand STABRITE cable made of 1-mm NbTi strands). The G-10 clamp prevented the cable in the secondary winding from motion due to electromagnetic forces.

The major limitation to the design was imposed by the

Manuscript received August 5, 2002. This work was supported by the U.S. Department of Energy.

N. Andreev, E. Barzi, S. Bhashyam, C. Boffo, D. R. Chichili, S. Yadav, I. Terechkine, A. V. Zlobin are with the Technical Division, Fermilab, Batavia, IL 60510, USA.

diameter of the Teslatron bore. The length of the sample splices (150 mm) is equal to the length of the splices in the dipole models. The length of the current transformer is about 200 mm and is limited by the length of the Teslatron test area.

The calculated electrical parameters of the transformer, such as inductance of the primary winding *L1*, inductance of the secondary winding *L2*, and mutual inductance *M*, are *L1* = 0.6 mH, *L2* = 0.23 μH, *M* = 7.3 μH.

A simple model of a superconducting current transformer can be derived in the assumption that it is fed by a power supply providing linear current ramp in the primary winding. The current in the secondary winding is fully defined by the primary current ramp rate, electrical parameters of the transformer, and resistance in the secondary circuit, which is mainly determined by the splice resistance. The relationship between secondary and primary currents is given by:

$$I_2 = \frac{M}{R_2} \cdot \frac{dI_1}{dt} \cdot (1 - e^{-t/\tau}), \qquad (1)$$

where the time constant $\tau = \frac{L_2}{R_2}$.

If $\frac{dI_1}{dt} = 0$ the current decay in the secondary winding in the approximation of a constant splice resistance can be found from the expression

$$I_2 = I_{2m} \cdot e^{-t/\tau} \quad . \qquad (2)$$

Where, I_{2m}, is the secondary current at the beginning of the decay. For I_{1max} = 1000 A, which is the maximum current currently available at SSTF, and for high primary current ramp rates, the secondary current of the transformer can theoretically reach $I_{2max} \approx 35$ kA. Although high current ramp rate in the primary coil may result in conductor AC heating, significant reduction of this rate would lead to substantial secondary current decay due to the splice resistance. To minimize this effect an optimal current ramp rate was used during each test run to maximize the secondary current.

III. SC Transformer Test Setup and Performance

The transformer was equipped with several voltage taps to monitor splice voltage and provide voltage signals for system protection and a spot heater to zero the current in secondary coil at the beginning of each transformer excitation. To measure the current in the secondary winding, a Rogowski-type probe was placed around the cable (Fig. 1). The total number of turns in the four-layer winding of the probe was 1400. The calculated relationship between the probe voltage and the current ramp rate in the cable was determined by:

$$U_{probe} = 1.45 \cdot 10^{-6} \cdot \frac{dI_2}{dt} \qquad (3)$$

The current in the secondary circuit can be found by integrating this voltage over the whole range of current sweep cycle. This was done, in our case, by an electronic integrator.

The performance of the transformer was tested with the insertion part made of NbTi cable similar to the cable in the regular part of secondary winding. The measured signals from the Rogowsky probe compared with the calculations are shown in Fig. 3. The measured current was quite consistent with the current calculated using (1) and (2).

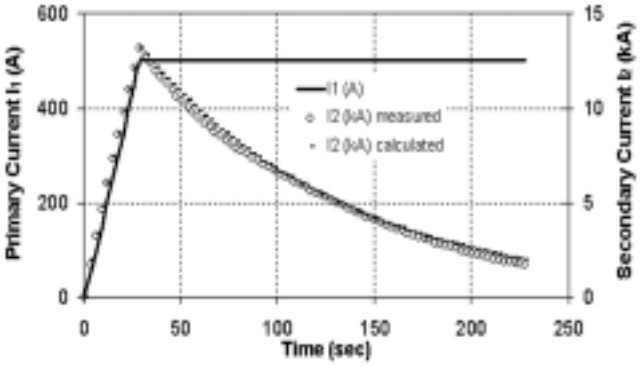

Fig. 3. Comparison of measured and calculated secondary currents.

The simplest transformer excitation cycle that uses fixed current ramp rate in the primary coil allows ramping the primary current up to ~800 A before quench conditions develop in the transformer primary winding. Although the maximum secondary current for the fast excitation ramp rate with this primary current is 28 kA, current decay reduces this value to about 20 kA. To increase the maximum achievable secondary current, modifications to this simple cycle needed to be made.

Two different approaches were investigated. The main idea behind these approaches was to reduce magnetic field on the strand that would allow further increase of the strand current. The straightforward way to increase the maximal current in the secondary winding is to use back ramp of the primary current following zeroing the current in the secondary winding after the initial forward ramp cycle. The secondary current can be set to zero by using the existing spot heater that increases strand temperature above the quench point or by waiting until the current decays to zero. During this back ramp of the primary current, magnetic field on the primary and secondary winding becomes smaller, that allows higher ramp rates and consequently results in higher current in the secondary winding. It was possible to increase the primary current to

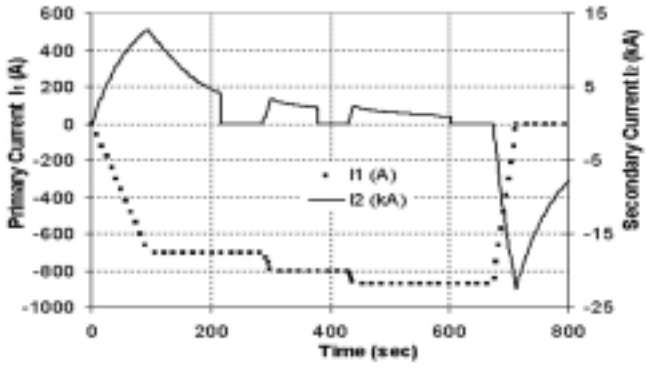

Fig. 4. Excitation diagram with three decay cycles in the secondary winding.

~900 A in a series of ramp-hold steps At each hold step, the

secondary current was set to zero by firing the spot heater after the current had decayed substantially. This process eliminated the secondary magnetic field contribution to the total field on the primary thereby permitting higher strand currents in the primary. The primary and secondary excitation cycle corresponding to this approach is shown in Fig. 4. As can be seen from Fig 4, it was possible to reach a maximum secondary current of about 22.5 kA following the ramp down of the primary at a high rate from 900 A.

The current-field (C-F) diagram of this cycle recording the position of working point (absolute values of the strand current and magnetic field) at each excitation step and the strand critical current for the primary and secondary are shown in Fig.5. As it follows from Fig. 5 (for the excitation cycle shown in Fig. 4), after the first current ramp when the secondary current decays to zero, the working point of the primary coil moves in the direction of lower magnetic field. Nevertheless, after the second and third ramps it moves in the opposite direction because the point of maximum magnetic field has moved from in between the two coils to the inside of the primary winding. Thus, after the second ramp, it is possible to ramp the primary current directly to its quench limit of about 900 A without additional cycling that involved setting the secondary current to zero.

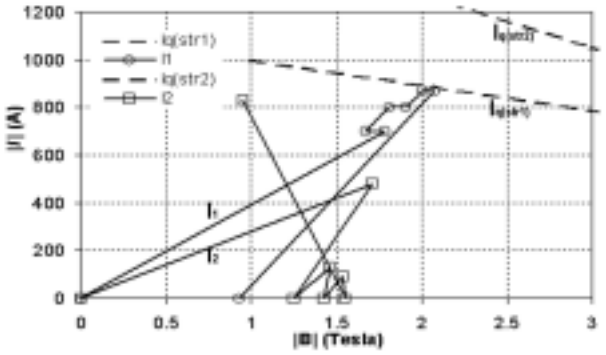

Fig. 5. Current-Field diagram corresponding to Fig. 4 excitation cycle.

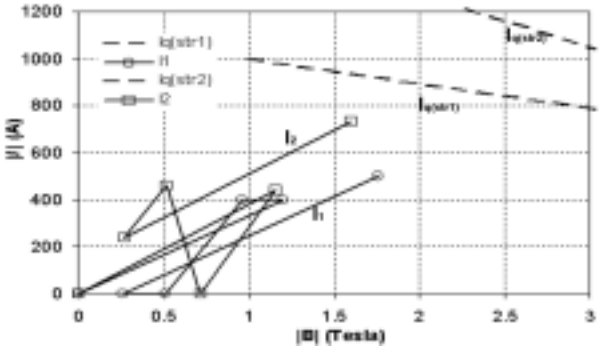

Fig. 6. Current-Field diagram for primary current polarity switching method.

The second method uses a slightly advanced approach. At the end of the simple cycle, similar to what is shown in Fig. 4, the polarity of the primary current is reversed and the forward ramp is repeated in the opposite direction. In this case the primary current swing can be doubled, resulting in a significant gain in the secondary current. This method illustrated by the C-F diagram shown in Fig. 6, can lead to further improvement of the transformer performance with secondary current increase up to 30 kA with the primary current not exceeding 800 A. To implement this, a current polarity switch is being added to the primary circuit.

IV. TEST RESULTS SUMMARY

The described SCT was used to study and optimize the current carrying capability and the resistance of the Nb_3Sn/NbTi cable splices used in Fermilab's high field dipole model magnets [1].

The splice resistance was measured on the decay part of the secondary current using (2) to fit the experimental data. Since the splice resistance is a function of current, it was always measured in the range of secondary currents of 13 - 22 kA. The resistance measured using this approach is the combined resistance of both the splices in the secondary circuit. Thus the splice resistance per side was determined as one-half the measured value. The splice current carrying capability studies were restricted by the transformer maximum current of 22 kA which exceeds the magnet short sample limit. Absence of quenches at this current was an acceptable criterion for the splice performance characterization.

The splice samples were fabricated using the same procedures as splices in the model magnets. The dependence of splice resistance on pressure applied on the cable during splicing is shown in Fig. 7. If pressure is below 15 MPa, the increase of resistance becomes quite sharp. The safe range of pressure is quite wide: from 20 to about 100 MPa. No strand degradation at high pressure was noticed, and no quench were observed due to the increased splice resistance. Repeated splicing work done on the same splice did not lead to irreversible cable degradation in any of these tests. This speaks for satisfactory reliability of the chosen splicing technique.

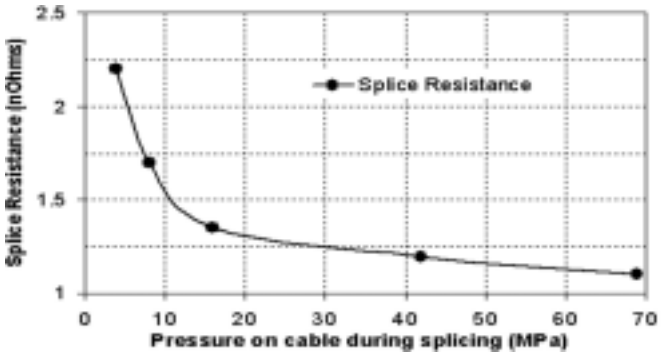

Fig. 7. Splice resistance as a function of applied pressure.

In order to study the effect of mechanical deformation of the Nb_3Sn cable during splicing on its current carrying capabilities, the reacted Nb_3Sn cable of the insertion part of the transformer was bent by pushing its end out of the plane of the cable ("easy-way" bend). The other end of the cable was clamped. Four dial indicators were placed at regular intervals along the length of the cable to record cable displacements. The first dial indicator was located 8 mm from the clamp while the fourth was located at the tip. The maximum tip deflection recorded was 17 mm which resulted in a deflection of 250 μm measured 8 mm from the clamp. After deformation, the cable

was unloaded, spliced back in the usual manner and re-tested. The cable curvature was calculated based on the displacement profile obtained from the dial indicator readings. Strain values, which are maximum in the vicinity of the clamp, were computed based on the cable curvature. The computed maximum strains were about 0.16% well below the limit of 0.3% [5]. The same experiment with a similar test setup was repeated by deforming the cable in the out of plane direction ("hard-way" bend). In this case, the tip was pushed out by 4 mm. Deforming the cable resulted in an increase of splice resistance to 1.6 nOhm, in case of the easy-way bend and 2.1 nOhm for hard-way bend, without any quenches in either case. Splices resistances could be restored to the original values of about 1.1 nOhm at 22 kA after re-splicing proving that there was no irreversible degradation due to the applied deformations. The cable deformations during this test were much larger than they usually were during magnet splice assembly.

The results of deformation testing indicated that deformation during splicing may not be the real cause for the poor quench performance of the magnet. That is why other concerns related to inadequate quench performance of the model magnets were investigated using the SCT. The list of potential causes includes effects of impregnation, cooling in the splice region and effects of differential thermal contractions of various materials in the splice area. A series of modifications to splice configuration were made accompanied by splice testing. Each previous test served as a baseline to the subsequent test. The virgin sample was tested before any modifications described below were made.

Test 1: Virgin sample –no modifications.

Test 2: Copper-made cable (150 mm long) is soldered to NbTi cable within the splice area.

Test 3: Nb_3Sn cable of the insertion part is glued to the ceramic pad using Hysol epoxy.

Test 4: The splice region was wrapped using 3 mil Kapton tape.

Test 5: Kapton thickness was increased to 6 mils.

Test 6: All layers of Kapton insulation were removed and the Nb_3Sn cable was completely separated (or de-bonded) from the ceramic pad. This test reproduce conditions of test 2.

Tests 2 and 3 allowed investigating the issue of differential thermal contraction between ceramic, the cable and the copper stabilizer. Tests 4 and 5 addressed splice cooling issues. In order to study the above effects, the Nb_3Sn cable was reacted using a heat treatment cycle that provided a relatively low cable critical current and possibility to observe quenches at currents below 20 kA.

The results from tests 1 through 6 are shown in Fig. 8. Several quench cycles were conducted for each of the tests. The solid line shows the change of average quench current from test to test. As it can be seen from this plot there is no noticeable effect of the above tests conditions on the critical current degradation. However, a significant scattering of the quench current values was noticed in tests 3, 4 and 5. Test 6 was performed to reproduce the conditions and results of test 2. The scatter in the quench data obtained from test 6 show that this variation could be attributed to the gluing of the Nb_3Sn cable to the ceramic pad.

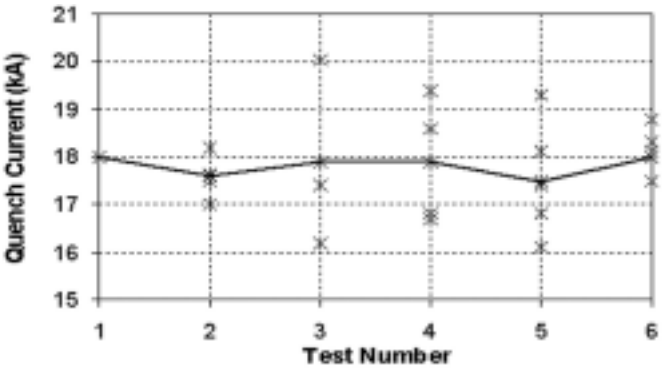

Fig. 8. Quench data from tests 1-6.

One additional sample was also spliced into the transformer and impregnated with CTD-101 epoxy as it was usually done in the dipole models. This configuration closely resembled the conditions present in the last model magnet and also did not show any above effects on the splice current carrying capability.

V. Conclusion

SCT has been designed and built to study the NbTi/Nb_3Sn splice technology and parameters. The performance of the transformer is in a good agreement with the theoretical predictions. The maximum current in the secondary circuit reaches 22.5 kA promising further increase after a polarity switch is introduced. The transformer is extensively used to optimize the splice fabrication technique providing quick test turn-around. The flexibility of the SCT architecture enables the investigation of other issues related to design of models magnets. This has been demonstrated by a series of SCT tests conducted to identify potential causes for observed quench performance of dipole model magnets.

References

[1] N. Andreev et al., "Development and Test of Single Bore Cosθ Nb_3Sn Dipole Models with Cold Iron Yoke", IEEE Transaction on Applied Superconductivity, v.12, No.1, March 2002, p.332.

[2] E. Barzi, C. Boffo, J. Ozelis, "Short Sample Jc Measurements at the SSTF", TD-98-057, FNAL, 10/13/98.

[3] G.B.J. Mulder et al., "A Convenient Method for Testing High-Current Superconducting Cables", Advances in Cryogenic Engineering, vol. 35, pp. 763-770, Plenum Press, New York, 1990.

[4] M. Kuchnir, "Electrical Resistance of Superconducting Cable Splices", Proc. of CEC/ICMC97, Portland, July 28-August 1, 1997.

[5] M. Wilson, Superconducting Magnets, Oxford Science Publications , 1982.